Figure S1

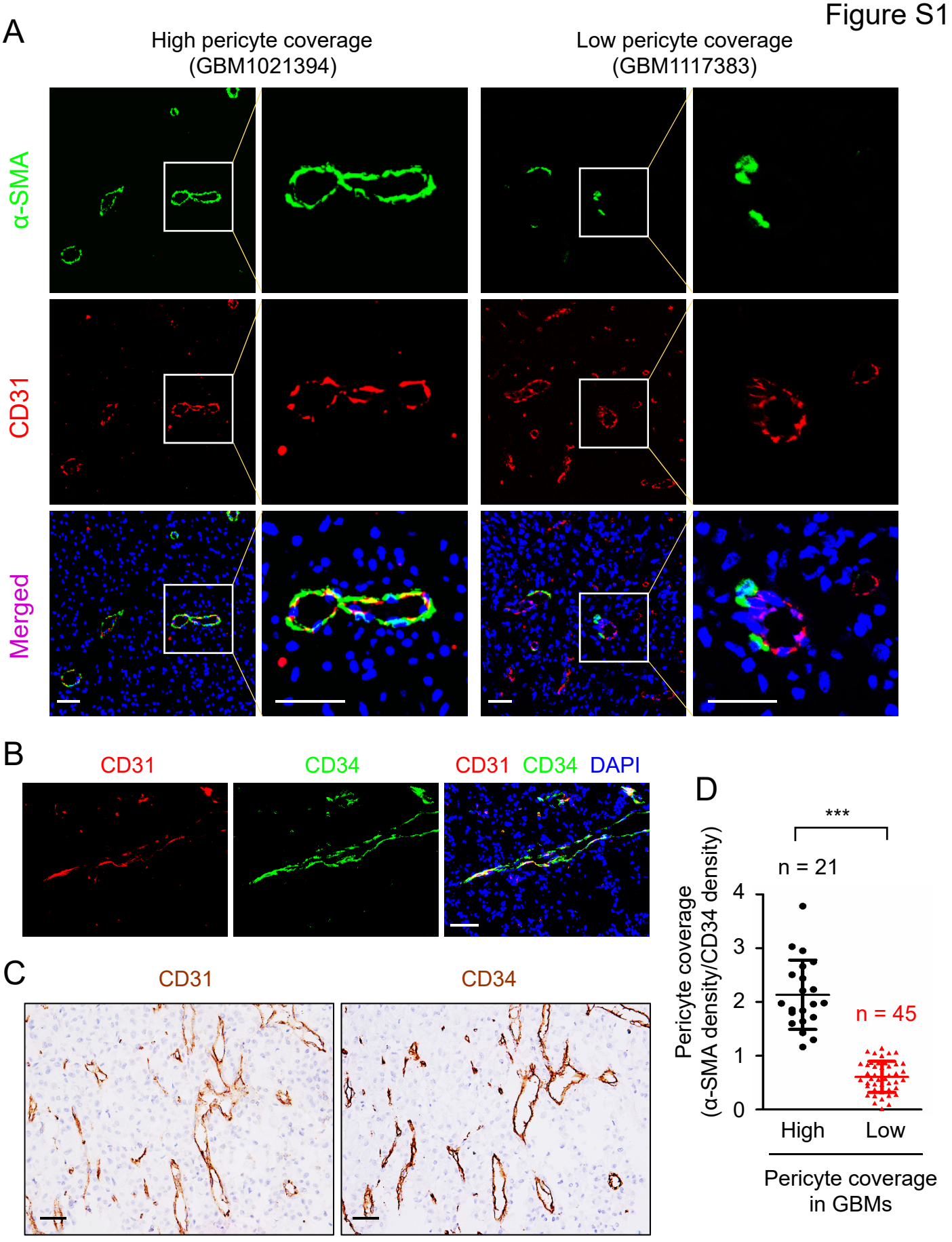
A
High pericyte coverage
(GBM1021394)
Low pericyte coverage
(GBM1117383)
α-SMA
CD31
Merged
B
CD31
CD34
CD31 CD34 DAPI
C
CD31
CD34
D
***
n = 21
n = 45
Pericyte coverage
(α-SMA density/CD34 density)
0
1
2
3
4
High
Low
Pericyte coverage
in GBMs

Figure S2

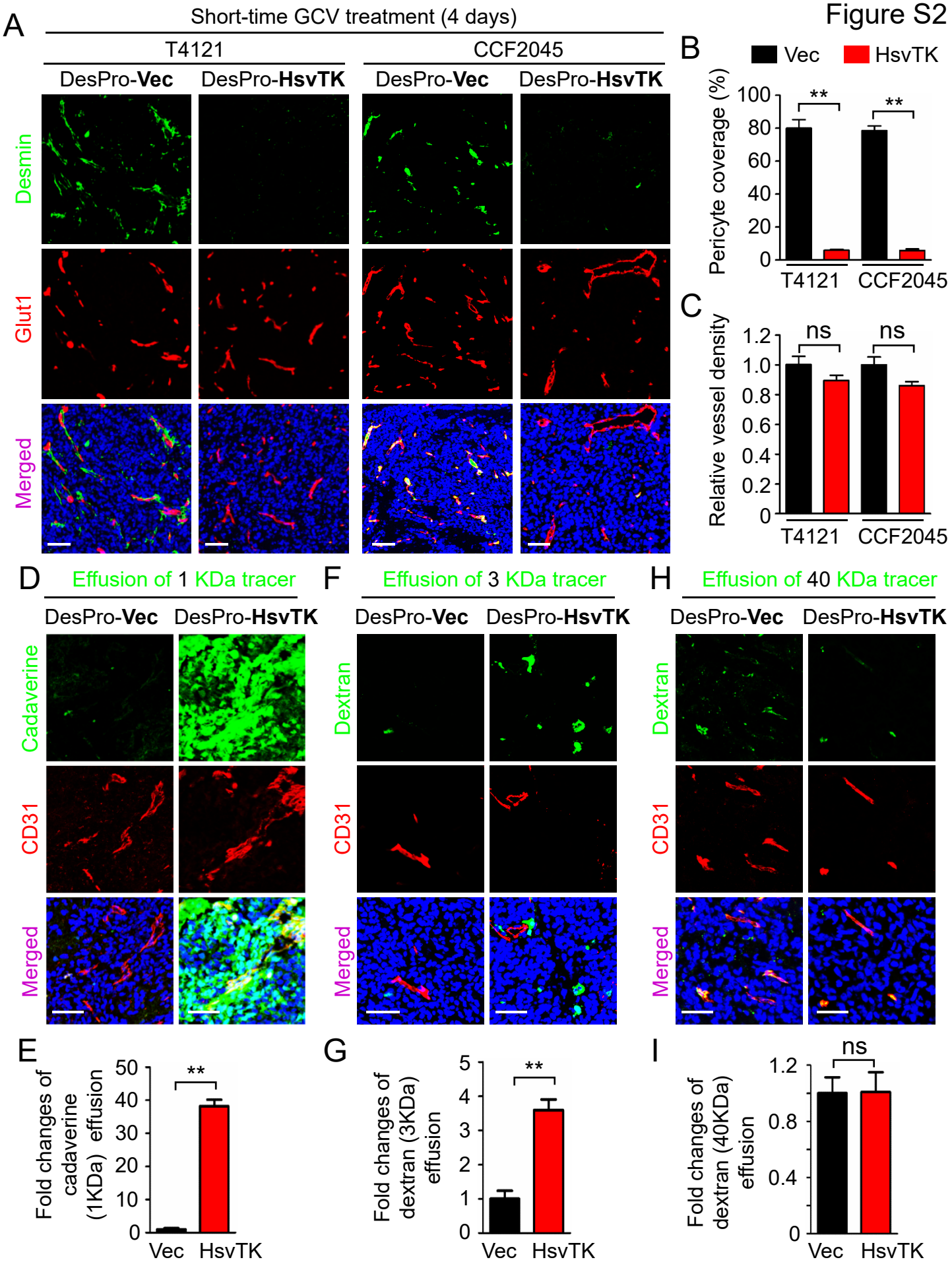
A
Short-time GCV treatment (4 days)
T4121
CCF2045
DesPro-Vec
DesPro-HsvTK
DesPro-Vec
DesPro-HsvTK
Desmin
Glut1
Merged
B
Vec
HsvTK
Pericyte coverage (%)
100
80
60
40
20
0
**
**
T4121
CCF2045
C
Relative vessel density
1.2
1.0
0.8
0.6
0.4
0.2
0
ns
ns
T4121
CCF2045
D
Effusion of 1 KDa tracer
DesPro-Vec
DesPro-HsvTK
Cadaverine
CD31
Merged
F
Effusion of 3 KDa tracer
DesPro-Vec
DesPro-HsvTK
Dextran
CD31
Merged
H
Effusion of 40 KDa tracer
DesPro-Vec
DesPro-HsvTK
Dextran
CD31
Merged
E
Fold changes of cadaverine (1KDa) effusion
50
40
30
20
10
0
**
Vec
HsvTK
G
Fold changes of dextran (3KDa) effusion
5
4
3
2
1
0
**
Vec
HsvTK
I
Fold changes of dextran (40KDa) effusion
1.2
0.8
0.4
0
ns
Vec
HsvTK

Figure S3

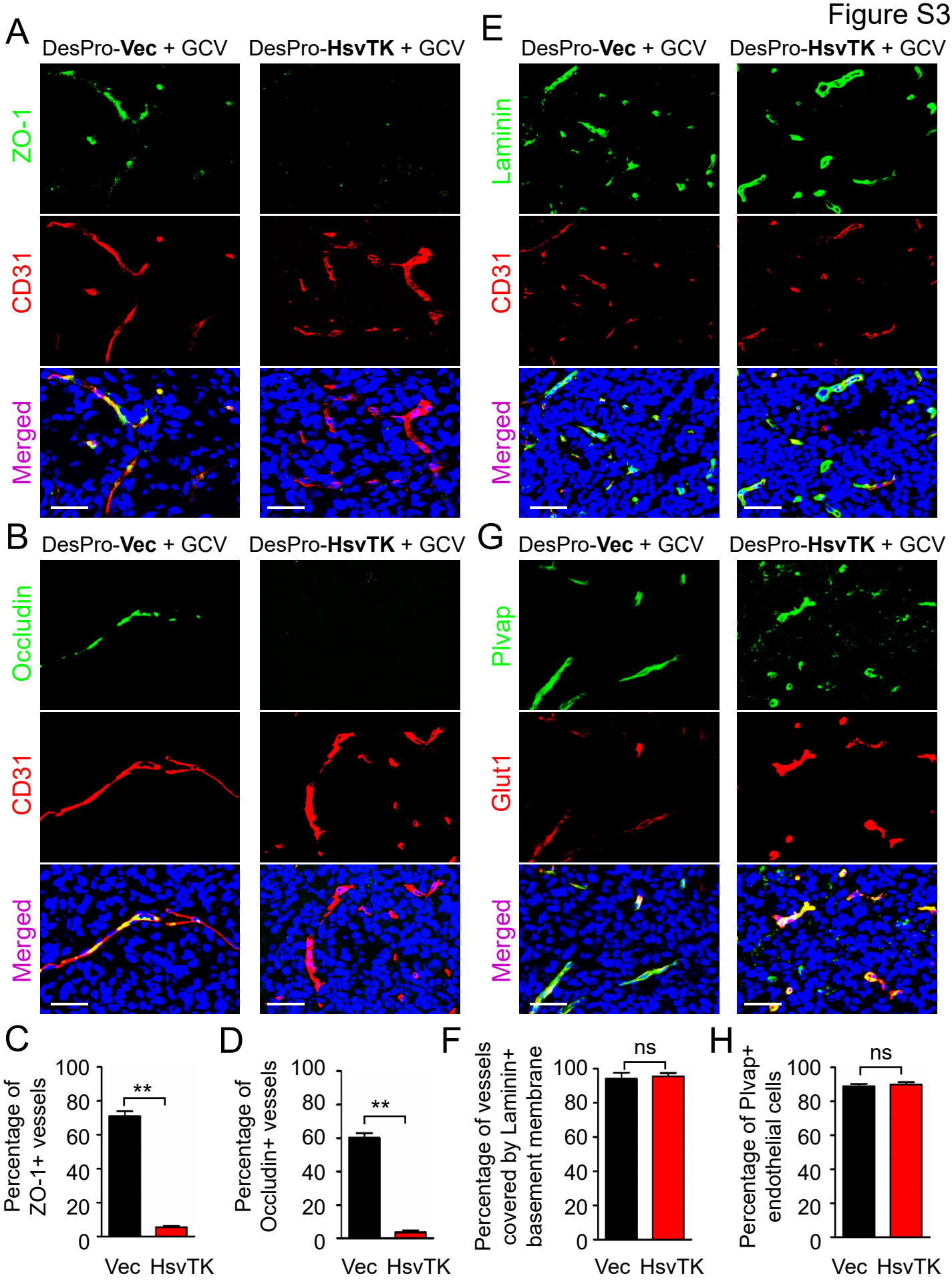
A
DesPro-Vec + GCV
DesPro-HsvTK + GCV
ZO-1
CD31
Merged
E
DesPro-Vec + GCV
DesPro-HsvTK + GCV
Laminin
CD31
Merged
B
DesPro-Vec + GCV
DesPro-HsvTK + GCV
Occludin
CD31
Merged
G
DesPro-Vec + GCV
DesPro-HsvTK + GCV
Plvap
Glut1
Merged
C
Percentage of ZO-1+ vessels
100
80
60
40
20
0
**
Vec
HsvTK
D
Percentage of Occludin+ vessels
100
80
60
40
20
0
**
Vec
HsvTK
F
Percentage of vessels covered by Laminin+ basement membrane
ns
100
80
60
40
20
0
Vec
HsvTK
H
Percentage of Plvap+ endothelial cells
ns
100
80
60
40
20
0
Vec
HsvTK

Figure S4

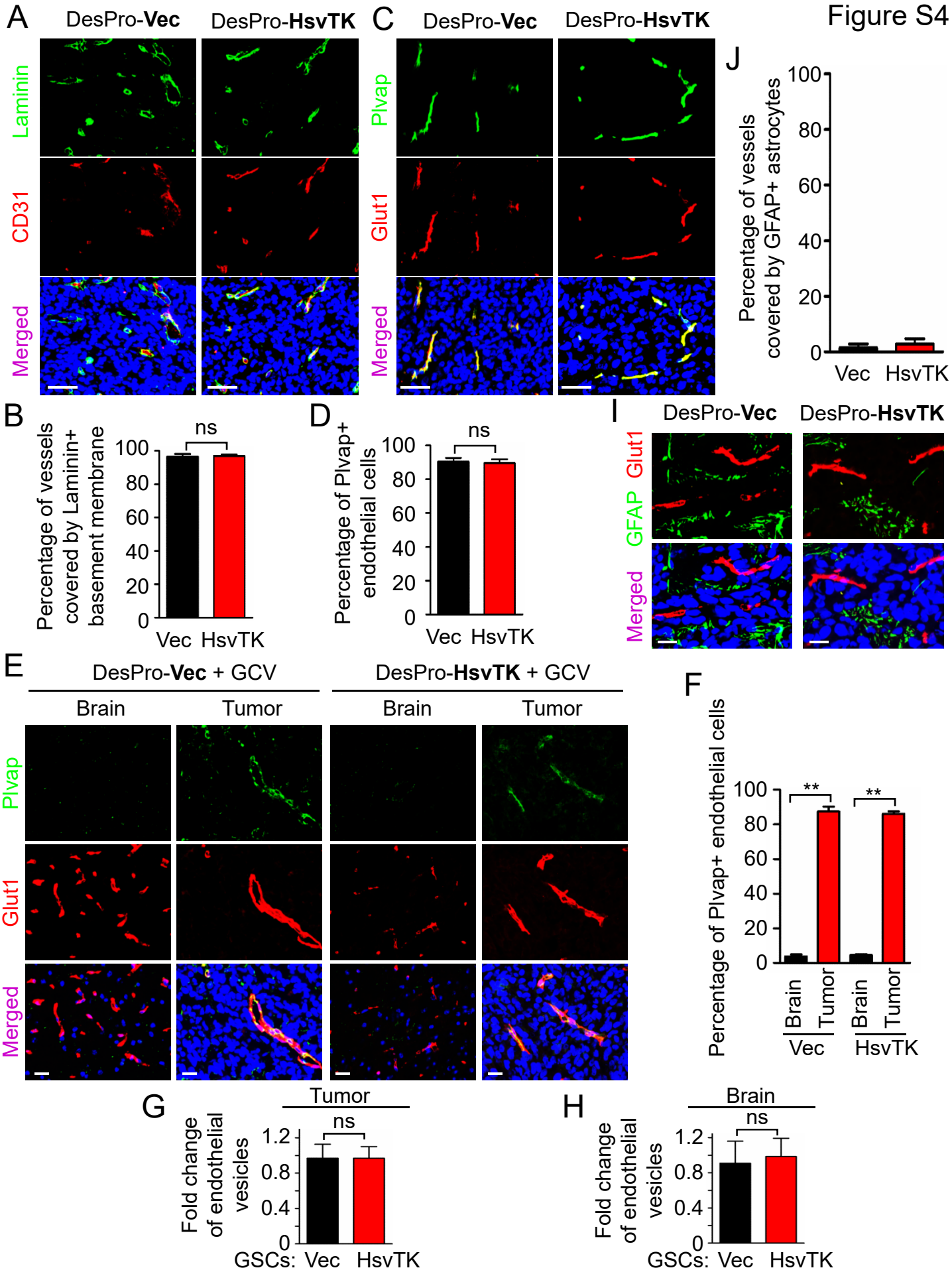
A
DesPro-Vec
DesPro-HsvTK
Laminin
CD31
Merged
C
DesPro-Vec
DesPro-HsvTK
Plvap
Glut1
Merged
J
Percentage of vessels covered by GFAP+ astrocytes
100
80
60
40
20
0
Vec
HsvTK
B
Percentage of vessels covered by Laminin+ basement membrane
ns
100
80
60
40
20
0
Vec
HsvTK
D
Percentage of Plvap+ endothelial cells
ns
100
80
60
40
20
0
Vec
HsvTK
I
DesPro-Vec
DesPro-HsvTK
Glut1
GFAP
Merged
E
DesPro-Vec + GCV
DesPro-HsvTK + GCV
Brain
Tumor
Brain
Tumor
Plvap
Glut1
Merged
F
Percentage of Plvap+ endothelial cells
**
**
100
80
60
40
20
0
Brain
Tumor
Brain
Tumor
Vec
HsvTK
G
Tumor
ns
Fold change of endothelial vesicles
1.2
0.8
0.4
0
GSCs: Vec
HsvTK
H
Brain
ns
Fold change of endothelial vesicles
1.2
0.8
0.4
0
GSCs: Vec
HsvTK

Figure S5

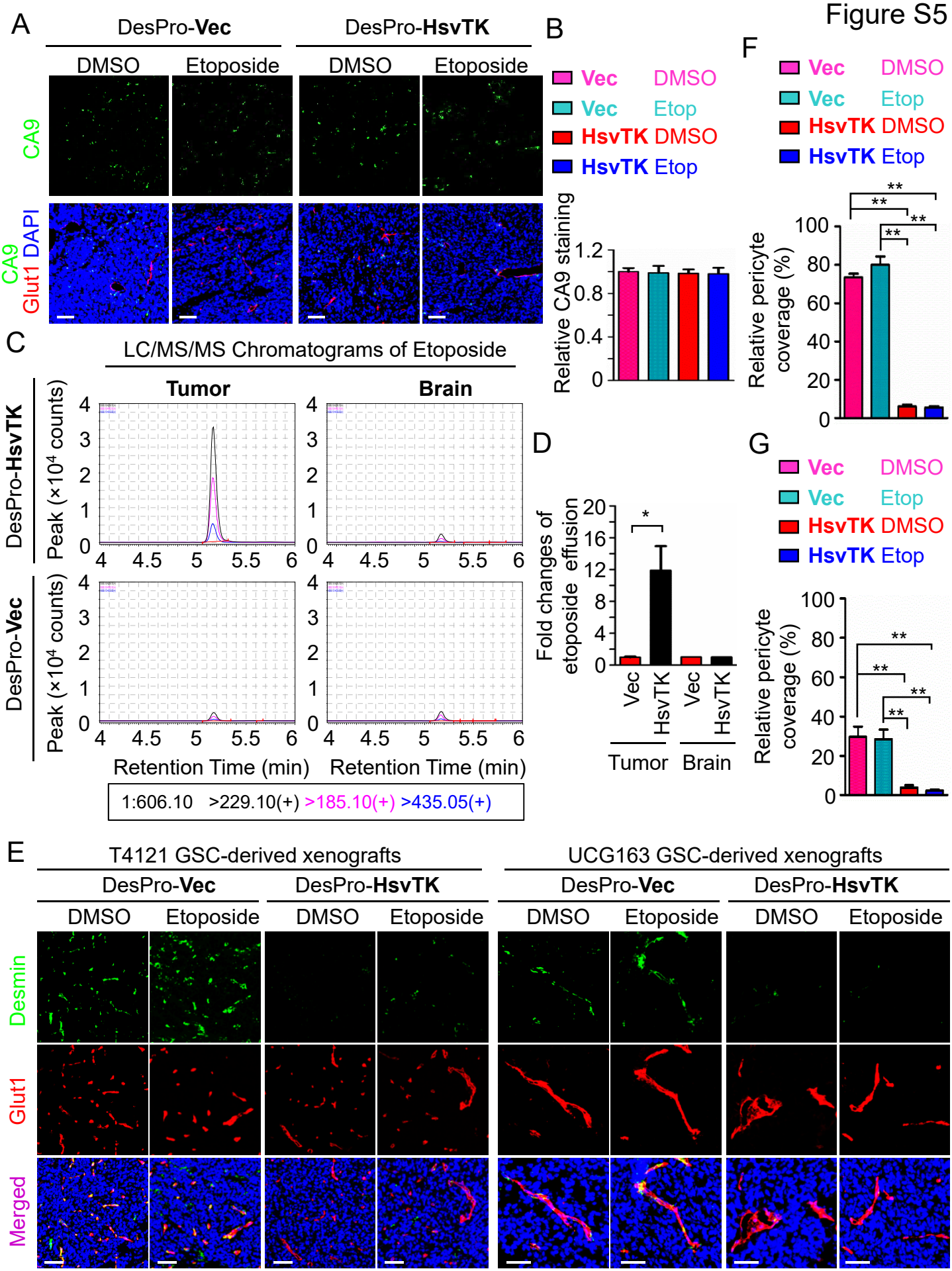
A
DesPro-Vec
DesPro-HsvTK
DMSO
Etoposide
DMSO
Etoposide
CA9
CA9 Glut1 DAPI
B
Vec DMSO
Vec Etop
HsvTK DMSO
HsvTK Etop
Relative CA9 staining
1.2
0.8
0.4
0
F
Vec DMSO
Vec Etop
HsvTK DMSO
HsvTK Etop
Relative pericyte coverage (%)
100
80
60
40
20
0
**
C
LC/MS/MS Chromatograms of Etoposide
Tumor
Brain
DesPro-HsvTK
DesPro-Vec
Peak (×10^4 counts)
4
3
2
1
0
4
4.5
5
5.5
6
Retention Time (min)
1:606.10 >229.10(+) >185.10(+) >435.05(+)
D
Fold changes of etoposide effusion
20
16
12
8
4
0
*
Vec
HsvTK
Vec
HsvTK
Tumor
Brain
G
Vec DMSO
Vec Etop
HsvTK DMSO
HsvTK Etop
Relative pericyte coverage (%)
100
80
60
40
20
0
**
E
T4121 GSC-derived xenografts
UCG163 GSC-derived xenografts
DesPro-Vec
DesPro-HsvTK
DesPro-Vec
DesPro-HsvTK
DMSO
Etoposide
DMSO
Etoposide
DMSO
Etoposide
DMSO
Etoposide
Desmin
Glut1
Merged

Figure S6

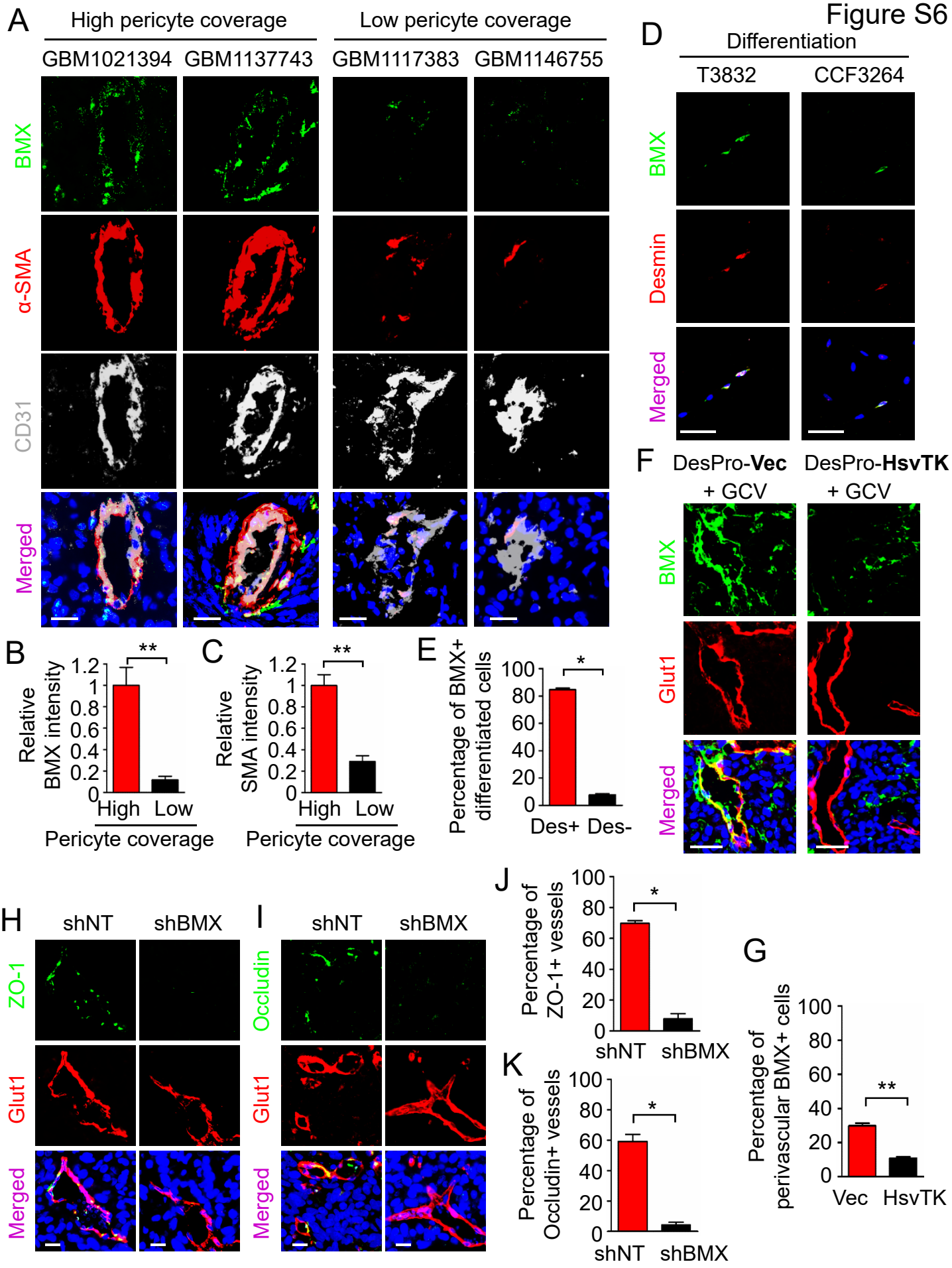
A
High pericyte coverage
Low pericyte coverage
GBM1021394
GBM1137743
GBM1117383
GBM1146755
BMX
α-SMA
CD31
Merged
B
Relative BMX intensity
**
High
Low
Pericyte coverage
C
Relative SMA intensity
**
High
Low
Pericyte coverage
E
Percentage of BMX+ differentiated cells
*
Des+
Des-
D
Differentiation
T3832
CCF3264
BMX
Desmin
Merged
F
DesPro-Vec + GCV
DesPro-HsvTK + GCV
BMX
Glut1
Merged
H
shNT
shBMX
ZO-1
Glut1
Merged
I
shNT
shBMX
Occludin
Glut1
Merged
J
Percentage of ZO-1+ vessels
*
shNT
shBMX
K
Percentage of Occludin+ vessels
*
shNT
shBMX
G
Percentage of perivascular BMX+ cells
**
Vec
HsvTK

Figure S7

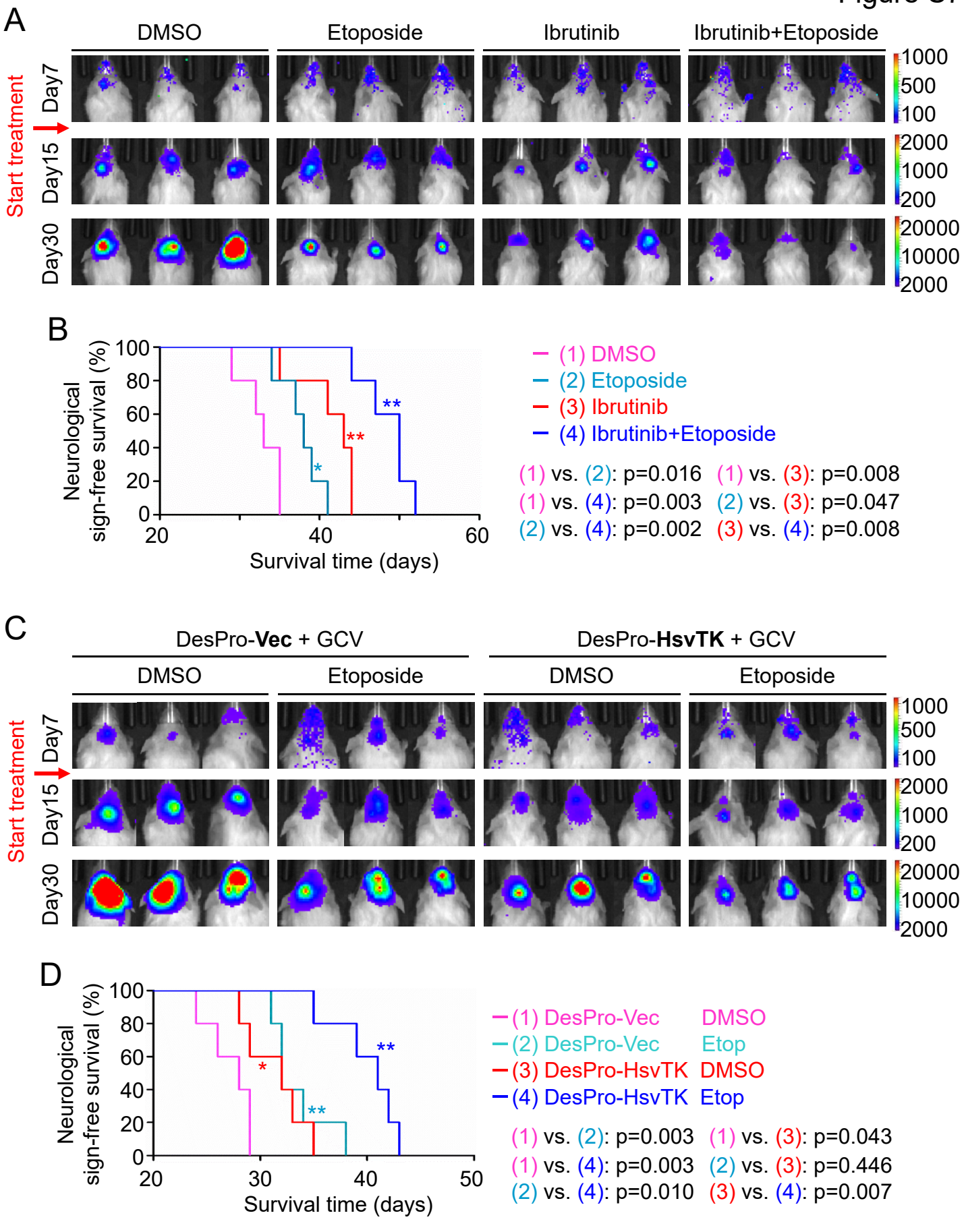
A
DMSO
Etoposide
Ibrutinib
Ibrutinib+Etoposide
Start treatment
Day7
Day15
Day30
1000
500
100
2000
1000
200
20000
10000
2000
B
Neurological sign-free survival (%)
100
80
60
40
20
0
20
40
60
Survival time (days)
*
**
**
(1) DMSO
(2) Etoposide
(3) Ibrutinib
(4) Ibrutinib+Etoposide
(1) vs. (2): p=0.016 (1) vs. (3): p=0.008
(1) vs. (4): p=0.003 (2) vs. (3): p=0.047
(2) vs. (4): p=0.002 (3) vs. (4): p=0.008
C
DesPro-Vec + GCV
DesPro-HsvTK + GCV
DMSO
Etoposide
DMSO
Etoposide
Start treatment
Day7
Day15
Day30
1000
500
100
2000
1000
200
20000
10000
2000
D
Neurological sign-free survival (%)
100
80
60
40
20
0
20
30
40
50
Survival time (days)
*
**
**
(1) DesPro-Vec DMSO
(2) DesPro-Vec Etop
(3) DesPro-HsvTK DMSO
(4) DesPro-HsvTK Etop
(1) vs. (2): p=0.003 (1) vs. (3): p=0.043
(1) vs. (4): p=0.003 (2) vs. (3): p=0.446
(2) vs. (4): p=0.010 (3) vs. (4): p=0.007

Table S1. Basic Information of GBM Patients in the Survival Study

Pathology ID	Gender	Age (years)	KPS	SMA/CD34 RATIO	Radio-therapy	Chemo-therapy	IDH1 mutation status	MGMT Status
201000727	Female	75	90	0.88	Yes	-	MU	+
201003492	Male	18	80	2.23	No	-	WT	-
201004805	Female	50	70	1.00	Yes	TMZ	WT	-
201009972	Female	26	40	0.47	Yes	ACNU	WT	-
201017276	Male	71	60	1.97	No	TMZ	NOS	-
201020927	Male	70	80	0.86	No	-	WT	-
201021387	Female	28	40	0.01	No	TMZ	MU	-
201021394	Male	73	80	2.51	Yes	ACNU	WT	-
201022270	Male	45	80	0.41	Yes	ACNU	MU	-
201023809	Female	69	80	0.19	No	-	WT	+
201033554	Male	48	90	3.78	No	TMZ	WT	-
201037273	Male	75	50	0.67	No	-	WT	-
201037481	Male	62	90	0.84	No	-	MU	-
201037501	Male	43	70	3.03	No	-	WT	-
201039610	Male	61	80	1.05	No	-	MU	-
201041295	Male	37	80	1.43	Yes	ACNU	MU	-
201042448	Male	42	70	0.78	No	-	WT	+
201042794	Female	60	80	0.83	No	ACNU	WT	-
201100535	Female	62	90	1.84	No	-	NOS	-
201100912	Male	44	80	1.80	No	ACNU	WT	-
201104873	Female	55	90	0.87	Yes	ACNU	WT	-
201109643	Male	64	70	2.75	Yes	ACNU	WT	-
201117383	Male	13	80	0.37	No	-	WT	-
201121887	Male	50	40	1.30	Yes	TMZ	WT	+
201124749	Female	67	70	0.57	No	-	NOS	-
201128852	Male	45	60	0.80	Yes	ACNU	WT	-
201129272	Male	62	80	1.86	No	-	NOS	+
201129281	Male	59	70	1.96	No	ACNU	WT	+
201130514	Female	41	60	2.21	No	TMZ	MU	+
201131949	Male	54	90	0.80	No	-	WT	-
201133838	Male	54	90	0.26	No	ACNU	WT	+
201136255	Male	60	70	0.51	Yes	ACNU	WT	+
201137743	Male	39	90	2.44	Yes	-	MU	-
201141427	Male	49	90	1.09	Yes	ACNU	WT	-
201142663	Female	72	80	1.64	No	ACNU	WT	-
201143172	Female	60	60	0.55	No	ACNU	NOS	+
201146755	Female	49	90	0.12	No	-	WT	+
201149841	Male	39	90	1.72	Yes	TMZ	WT	+

201202462	Male	43	60	0.64	No	-	WT	+
201202463	Male	68	80	0.64	No	-	MU	+
201203703	Female	72	70	0.44	No	ACNU	WT	+
201209010	Female	41	90	0.68	Yes	ACNU	MU	-
201211305	Female	55	70	1.05	No	-	WT	-
201211306	Male	66	80	1.06	No	-	WT	-
201212593	Male	47	80	2.66	Yes	ACNU	WT	-
201216972	Male	30	70	0.49	Yes	ACNU	MU	-
201218411	Male	33	90	0.71	Yes	ACNU +TMZ	WT	+
201219358	Female	54	50	1.08	Yes	TMZ	NOS	-
201231082	Male	34	80	1.60	No	-	WT	-
201238753	Male	32	80	0.56	Yes	TMZ	MU	-
201241585	Female	45	70	0.87	Yes	TMZ	WT	+
201246830	Male	53	80	1.16	Yes	-	WT	-
201306934	Female	21	90	0.28	No	-	WT	-
201307204	Male	32	90	1.98	Yes	TMZ	WT	-
201317259	Male	55	90	0.37	No	-	NOS	+
201319360	Female	64	80	0.58	Yes	TMZ	WT	-
201327305	Female	56	80	0.33	Yes	TMZ	WT	+
201329927	Female	64	70	0.26	Yes	TMZ	MU	+
201330615	Female	23	70	0.09	No	TMZ	MU	+
201333366	Male	39	80	0.47	Yes	TMZ	WT	+
201336128	Male	56	90	0.26	No	-	WT	-
201400034	Male	47	80	2.95	No	-	MU	+
201401749	Female	44	90	0.63	No	TMZ	MU	+
201403625	Male	45	90	0.85	Yes	TMZ	NOS	+
201405593	Male	67	80	0.55	Yes	TMZ	MU	+
201423279	Female	64	90	0.50	Yes	TMZ	WT	-

KPS: Karnofsky Performance Scale Index indicates the functional impairment of the patients. The lower score stands for the worse status of the patient.
TMZ: Temozolomide
ACNU: Nimustine
IDH1 status: WT, wild type; MU, mutant type; NOS, not otherwise specified.

The table contains basic information of the GBM patients in the survival study, including the pathology ID, gender, age, KPS index, pericyte coverage (the ratio of SMA/CD34 density in each GBM), radiotherapy situation (yes or no), drugs used for chemotherapy, IDH1 mutation status and the MGMT status.

SUPPLEMENTARY FIGURE LEGENDS

Figure S1. Human GBM Tumors Display Varied Pericyte Coverage on Vessels, Related to Figure 1.

(A) Immunofluorescent analyses of the tumor pericyte marker α-SMA (in green) and the endothelial marker CD31 (in red) showing the varied pericyte coverage in different human primary GBMs. Frozen sections of GBM specimens were immunostained for α-SMA and CD31 and then counterstained with DAPI (in blue). Representative images were shown for the high pericyte coverage (left panel) and the low pericyte coverage (right panel) in two typical cases of GBM surgical specimens. Scale bar represents 80μm.

(B) Immunofluorescent staining of the endothelial cell markers CD31 (in red) and CD34 (in green) to mark tumor vessels on frozen sections of a human primary GBM. Both CD31 and CD34 marked the same vessels in the GBM tumor. Scale bar represents 80μm.

(C) Immunohistochemical staining of the endothelial cell marker CD31 (left panel) or CD34 (right panel) to label tumor vessels on consecutive FFPE sections in a human primary GBM. Sequential FFPE sections of a human GBM were immunostained with anti-CD31 or anti-CD34 antibody. The anti-CD34 antibody showed stronger staining than the anti-CD31 antibody in the paraffin sections. Scale bar represents 20μm.

(D) Dot plots of pericyte coverage in GBM tumors with high or low pericyte coverage from different patients. Pericyte coverage was defined as the ratio of α-SMA intensity (pericyte density) to the CD34 intensity (endothelial density) detected in immunohistochemical staining. The average pericyte coverage of all GBMs was used as the cut-off to divide GBM patients into high and low pericyte coverage groups. These two groups showed a significant difference in their

pericyte coverage. ***, $p < 0.001$ (n = 45 for low pericyte coverage, n = 21 for high pericyte coverage, $p < 0.001$, mean ± s.d.; Mann Whitney test).

Figure S2. Disruption of GSC-derived Pericytes Increased Vascular Permeability in GBM Xenografts, Related to Figure 2.

(A) Immunofluorescent analyses of the pericyte marker Desmin (in green) and the endothelial marker Glut1 (in red) in GBM xenografts derived from T4121 or CCF2045 GSCs transduced with DesPro-HsvTK or DesPro-Vec after GCV treatment for 4 days. Frozen sections of the xenografts were immunostained with specific antibodies against Desmin and Glut1 and counterstained with DAPI (in blue) (n = 5 tumors for each group). GCV treatment for a short time (4 days) resulted in a reduction of pericytes in the tumors derived from DesPro-HsvTK-transduced GSCs relative to control tumors derived from DesPro-Vec-transduced GSCs, but the overall vessel density was not affected by the short-term disruption of pericytes. Scale bar represents 80μm.

(B) Statistical analysis of pericyte coverage in xenografts derived from the GSCs transduced with DesPro-Vec or DesPro-HsvTK after GCV treatment described in (A). Pericyte coverage was significantly reduced in xenografts derived from the GSCs transduced with DesPro-HsvTK relative to xenografts derived from the GSCs transduced with DesPro-Vec after GCV treatment for 4 days. (n = 5 tumors for each group, **, $p < 0.01$, mean ± s.e.m.; Mann Whitney test).

(C) Statistical quantification of vessel density in xenografts derived from GSCs transduced with DesPro-Vec or DesPro-HsvTK after GCV treatment described in (A). No significant difference in vessel density was observed between tumors derived from GSCs transduced with DesPro-Vec or DesPro-HsvTK after GCV treatment for 4 days. Vessel density was analyzed with Image J. (n

= 5 tumors for each group; mean ± s.e.m.; ns, $p > 0.01$; Mann Whitney test).

(D) Fluorescent analysis of small molecule effusion using the autonomous fluorescent tracer cadaverine (in green, 1kDa) and immunofluorescent staining of the endothelial marker CD31 (in red) in GBM xenografts derived from the GSCs (CCF2045) transduced with DesPro-HsvTK or DesPro-Vec after GCV treatment. Substantial cadaverine effusion into tumor tissues was detected in xenografts derived from the GSCs transduced with DesPro-HsvTK after GCV treatment for 4 days to disrupt the GSC-derived pericytes. However, negligible cadaverine signal was detected in the control xenografts derived from the GSCs transduced with DesPro-Vec after the GCV treatment. This indicates that disruption of GSC-derived pericytes increased vascular permeability in the tumor. Scale bar represents 80μm.

(E) Statistical quantification of cadaverine effusion into xenografts derived from the GSCs transduced with DesPro-HsvTK or DesPro-Vec control after GCV treatment as described in (D). Cadaverine effusion into tumors was determined by cadaverine positive areas normalized to vessel density. A significant increase of cadaverine effusion was detected in xenografts derived from the DesPro-HsvTK-transduced GSCs relative to xenografts derived from the DesPro-Vec-transduced GSCs after GCV treatment. (n = 5 tumors for each group; **, $p < 0.01$; mean ± s.e.m.; Mann Whitney test).

(F) Fluorescent analysis of the effusion of medium-sized molecules with the autonomous fluorescent tracer Alexa Fluor 488 dextran-3kDa (in green) and immunofluorescent staining of the endothelial marker CD31 (in red) in xenografts derived from the GSCs (CCF2045) transduced with DesPro-HsvTK or DesPro-Vec control after GCV treatment. An increase of the dextran signal was detected in xenografts derived from the DesPro-HsvTK-transduced GSCs relative to the DesPro-Vec-transduced GSCs after GCV treatment. Scale bar represents 80μm.

(G) Statistical quantification of the effusion of medium-sized molecules (Alexa Fluor 488 dextran-3kDa) into xenografts derived from the GSCs transduced with DesPro-HsvTK or DesPro-Vec control after GCV treatment described in (F). Dextran effusion was determined by dextran positive areas normalized to vessel density. The effusion of the 3kDa dextran was increased in xenografts derived from the DesPro-HsvTK-transduced GSCs relative to xenografts derived from the DesPro-Vec-transduced GSCs after GCV treatment. (n = 5 tumors for each group; **, $p < 0.01$; mean ± s.e.m.; Mann Whitney test).

(H) Fluorescent analysis of the effusion of large molecules with the autonomous fluorescent tracer Alexa Fluor 488 dextran-40kDa (in green) and immunofluorescent staining of the endothelial marker CD31 (in red) in xenografts derived from the GSCs (CCF2045) transduced with DesPro-HsvTK or DesPro-Vec control after GCV treatment. Negligible dextran signal was detected in both xenografts derived from the GSCs transduced with DesPro-HsvTK or DesPro-Vec after GCV treatment, indicating that disruption of GSC-derived pericytes did not increase effusion of large molecules into GBM tumors. Scale bar represents 80μm.

(I) Statistical quantification of the effusion of large molecules (dextran-40kDa) into xenografts derived from the GSCs transduced with DesPro-HsvTK or DesPro-Vec control after GCV treatment described in (H). Dextran effusion was determined by dextran positive areas normalized to vessel density. No difference in dextran effusion was detected in xenografts derived from the DesPro-HsvTK-transduced GSCs relative to xenografts derived from the DesPro-Vec-transduced GSCs after the GCV treatment, indicating that disruption of GSC-derived pericytes could not increase effusion of large molecule into tumor tissues (n = 5 tumors for each group; ns, $p > 0.05$; mean ± s.e.m.; Mann Whitney test).

Figure S3. Elimination of GSC-derived Pericytes Disrupted the BTB Tight Junctions but Not Other BTB Components, Related to Figure 3.

(A and B) Immunofluorescent analyses of the tight junction markers ZO-1 (A) and Occludin (B) (in green) and the vessel marker CD31 (in red) in xenografts derived from the GSCs (CCF2045) transduced with DesPro-Vec or DesPro-HsvTK after GCV treatment. ZO-1 or Occludin signal on tumor vessels was reduced in xenografts derived from the DesPro-HsvTK-transduced GSCs relative to the control xenografts derived from the DesPro-Vec-transduced GSCs. Scale bar represents 80μm.

(C and D) Statistical quantification of (A) and (B) to determine ZO-1 (C) and Occludin (D) staining signals on vessels in xenografts derived from the GSCs transduced with DesPro-HsvTK or DesPro-Vec after GCV treatment. The percentage of ZO-1-positive or Occludin-positive vessels was determined by the numbers of ZO-1-positive or Occludin-positive cells normalized to the numbers of CD31-positive cells (n = 5 tumors for each group; **, $p < 0.01$; mean ± s.e.m.; Mann Whitney test).

(E) Immunofluorescent staining of the vascular basement membrane marker Laminin (in green) and the endothelial marker CD31 (in red) in xenografts derived from the GSCs (CCF2045) transduced with DesPro-Vec or DesPro-HsvTK after GCV treatment. Vessels in both groups of xenografts were covered with basement membrane, indicating that disruption of GSC-derived pericytes did not impact integrity of vascular basement membrane. Scale bar represents 40μm.

(F) Statistical quantification of the vessel basement membrane in (E). Vascular basement membrane was quantified according to the percentage of CD31-positive vessels covered by Laminin-positive basement membrane. Vascular basement membrane coverage had no difference between xenografts derived from the DesPro-HsvTK-transduced GSCs and those derived from

DesPro-Vec-transduced GSCs. (n = 5 tumor for each group; ns, $p > 0.05$; mean ± s.e.m.; Mann Whitney test).

(G) Immunofluorescent analysis of the transcytosis marker Plvap (in green) and the endothelial marker Glut1 (in red) in xenografts derived from the GSCs (CCF2045) transduced with DesPro-Vec or DesPro-HsvTK. Substantial Plvap expression was detected in endothelial cells in both groups of the xenografts, indicating an intact transcytosis across endothelial cells on vessels with or without pericyte disruption. Scale bar represents 40μm.

(H) Statistical quantification of Plvap levels in endothelial cells in (G). Percentage of endothelial cells (Glut1+) positive for Plvap was quantified. No difference of Plvap intensity was found between xenografts derived from the GSCs transduced with DesPro-Vec and DesPro-HsvTK after GCV treatment, indicating that disruption of GSC-derived pericytes did not impact transcytosis in endothelial cells. (n = 5 tumors for each group; ns, $p > 0.05$; mean ± s.e.m.; Mann Whitney test).

Figure S4. Disruption of GSC-derived Pericytes Did Not Impact Other BTB Components except for Tight Junctions, Related to Figure 3.

(A) Immunofluorescent analysis of the vascular basement membrane marker Laminin (in green) and the endothelial marker CD31 (in red) in xenografts derived from the GSCs (T4121) transduced with DesPro-Vec or DesPro-HsvTK after GCV treatment. Vessels in both groups of xenografts were covered with similar basement membrane, indicating that disruption of GSC-derived pericytes did not impact integrity of vascular basement membrane. Scale bar represents 40μm.

(B) Statistical quantification of the vessel basement membrane in (A). Vascular basement

membrane was quantified according to the percentage of CD31-positive vessels covered by Laminin-positive basement membrane. Vascular basement membrane coverage had no difference between xenografts derived from the DesPro-HsvTK-transduced GSCs and the DesPro-Vec-transduced GSCs. (n = 5 tumors for each group; ns, $p > 0.05$; mean ± s.e.m.; Mann Whitney test).

(C) Immunofluorescent staining of the transcytosis marker Plvap (in green) and the endothelial marker Glut1 (in red) in xenografts derived from the GSCs (T4121) transduced with DesPro-Vec or DesPro-HsvTK after GCV treatment. Substantial Plvap expression was detected in endothelial cells in both groups of the xenografts, indicating intact transcytosis across endothelial cells with or without disruption of pericytes. Scale bar represents 40μm.

(D) Statistical quantification of Plvap signals in endothelial cells in (C). Percentage of endothelial cells (Glut1+) positive for Plvap was quantified. No difference of Plvap intensity was found between xenografts derived from the GSCs transduced with DesPro-Vec and DesPro-HsvTK, indicating that disruption of GSC-derived pericytes did not impact transcytosis in endothelial cells. (n = 5 tumors for each group; ns, $p > 0.05$; mean ± s.e.m.; Mann Whitney test).

(E) Immunofluorescent analysis of the transcytosis marker Plvap (in green) and the endothelial marker Glut1 (in red) in xenografts derived from the GSCs (T4121) transduced with DesPro-Vec or DesPro-HsvTK and in the matched normal brain tissues after GCV treatment. Substantial Plvap expression was detected in endothelial cells in tumor tissues but not in normal brain tissues. Scale bar represents 40μm.

(F) Statistical quantification of Plvap signals in endothelial cells. Percentage of endothelial cells (Glut1+) positive for Plvap was quantified. Plvap intensity was significantly increased in tumors than in matched normal brain tissues. (n = 5 tumors for each group; **, $p < 0.01$; mean ± s.e.m.; Mann Whitney test).

(G and H) Statistical quantification to show the fold change of the endothelial vesicle number in endothelial cells on tumor vessels (G) and brain vessels (H) after disruption of tumor neoplastic pericytes. T4121 GSCs transduced with DesPro-Vec or DesPro-HsvTK were injected into mouse brains. Twenty days after GSC implantation, mice bearing tumors were treated with GCV for 5 days. Vascular ultrastructure of tumor tissue and the corresponding normal brain tissue were analyzed by transmission electron microscopy. For quantification of endothelial vesicles, the small vesicles (20 to 100 nm in diameter) inside vascular endothelial cells, which appeared as circular organelles having lighter electron density within, were counted and quantified. No significant change in the numbers of transcytotic vesicles was observed in tumor or brain vascular endothelial cells after disruption of tumor neoplastic pericytes. (n = 12 vessels for each group; ns, $p > 0.05$; mean ± s.e.m.; Mann Whitney test).

(I) Immunofluorescent analysis of the astrocyte marker GFAP (in green) and the endothelial marker Glut1 (in red) in xenografts derived from the GSCs (T4121) transduced with DesPro-Vec or DesPro-HsvTK after GCV treatment. Blood vessels in both groups of xenografts showed little contact with astrocytes. Scale bar represents 20μm.

(J) Statistical quantification of the vessels covered by astrocyte end-feet in (I). Astrocyte end-feet coverage on vessels was determined by the percentage of endothelial cells (Glut1+) in contact with astrocyte (GFAP+) end-feet. Little astrocyte end-feet coverage was detected in either groups of the xenografts. No difference of the astrocyte end-feet was detected between xenografts derived from the DesPro-HsvTK-transduced GSCs and the DesPro-Vec-transduced GSCs after GCV treatment (n = 5 tumors for each group; ns, $p > 0.05$; mean ± s.e.m.; Mann Whitney test).

Figure S5. Pulse Disruption of Neoplastic Pericytes Maintained Vascular Perfusion but

Increased Etoposide Effusion into Tumor Tissues, Related to Figure 4.

(A) Immunofluorescent analysis of the hypoxia marker CA9 (in green) to detect changes in vascular perfusion and analysis of the endothelial cell marker Glut1 (in red) to label vessels in xenografts derived from T4121 GSCs transduced with DesPro-Vec or DesPro-HsvTK after GCV in combination with etoposide treatment. 5 days after GSC implantation, mice bearing the tumors were treated with pulse administration of GCV (1mg/20g) for two consecutive days with a two-day interval. Etoposide (60μg/20g) was administered daily. 25 days post-transplantation, xenografts in mouse brains were harvested for the analysis. Scattered CA9 signals at the similar intensity were detected in tumors from all groups, indicating that pulse disruption of GSC-derived pericytes by such GCV treatment did not affect vascular perfusion. Scale bar represents 80μm.

(B) Statistical quantification of (A) shows the relative CA9 intensity in tumors from all four treatment groups. No significant change of CA9 intensity was detected in tumors with or without the pulse disruption of GSC-derived pericytes, suggesting that the vascular perfusion was maintained after the pulse disruption of the neoplastic pericytes. (n = 5 tumors for each group; mean ± s.e.m.; Mann Whitney test).

(C) Representative LS/MS/MS chromatograms of etoposide concentrations in tumor tissues and the matched normal brain tissues in mice bearing GBM xenografts derived from T4121 GSCs transduced with DesPro-HsvTK or DesPro-Vec control after GCV treatment. 20 days after transplantation of GSCs, mice were treated with GCV for 4 days followed by intraperitoneal injection of etoposide (60μg/20g). 2 hours after etoposide injection, mice were anaesthetized, perfused with PBS, and sacrificed. Tumors and the corresponding normal brain tissues were collected, homogenized in PBS, and subjected to LS/MS/MS chromatography. An obvious

increase of etoposide drug signal was detected in tumor tissues relative to the matched normal brain tissues after disruption of GSC-derived neoplastic pericytes (upper panel). Similar etoposide signals were detected in tumor tissues and matched normal brain tissues without disruption of the neoplastic pericytes (lower panel).

(D) Statistical analysis of the LS/MS/MS chromatography to show the relative fold changes of etoposide effusion into tumor tissues and the matched brain tissues in mice bearing GBMs derived from T4121 GSCs transduced with DesPro-Vec or DesPro-HsvTK after GCV treatment. Selective disruption of GSC-derived neoplastic pericytes significantly increased etoposide effusion into tumor tissues but not into the matched normal brain tissues. (n = 5 mice for each group; *, $p < 0.05$; mean ± s.e.m.; Mann Whitney test).

(E) Immunofluorescent analysis of the pericyte marker Desmin (in green) and the endothelial marker Glut1 (in red) in xenografts derived from GSCs (T4121 and UCG163) transduced with DesPro-HsvTK or DesPro-Vec control after treatment with GCV in combination with etoposide or DMSO. Mice bearing the GSC-derived xenografts were treated with pulsed-dose GCV plus etoposide or DMSO. Pericyte coverage was relatively high in the T4121 GSC-derived xenografts and relatively low in the UCG163 GSC-derived xenografts. However, in both tumors, GCV treatment disrupted vascular pericytes in xenografts derived from the DesPro-HsvTK-transduced GSCs but not in the xenografts derived from the DesPro-Vec-transduced GSCs, confirming selective targeting of GSC-derived pericytes expressing HsvTK by GCV treatment. Scale bar represents 80μm.

(F and G) Statistical quantification of pericyte coverage in xenografts derived from the T4121 GSCs (F) or CCF2045 GSCs (G) transduced with DesPro-Vec or DesPro-HsvTK after pulsed-dose GCV plus etoposide or DMSO treatment described in (E). Pericyte coverage was

significantly reduced in xenografts derived from GSCs transduced with DesPro-HsvTK relative to xenografts derived from the GSCs transduced with DesPro-Vec control after GCV treatment. (n = 5 tumors for each group; **, $p < 0.01$, mean ± s.e.m.; Mann Whitney test).

Figure S6. BMX Is Highly Expressed in GSC-derived Pericytes and Targeting BMX Disrupted the BTB Tight Junctions in GBM Tumors, Related to Figures 5 and 6.

(A) Immunofluorescent analysis of BMX (in green), the tumor pericyte marker α-SMA (in red), and the endothelial cell marker CD31 (in gray) in human primary GBM tumors with high and low pericyte coverage. BMX staining was detected in the vascular pericytes (α-SMA+) on tumor vessels in GBMs. Relatively high BMX expression was detected in GBM specimens with high pericyte coverage relative to the tumor specimens with low pericyte coverage. Scale bar represents 40μm.

(B and C) Statistical quantification of (A) shows the relative intensity of BMX (B) and α-SMA (C) signals in GBMs with high or low pericyte coverage. A significantly higher expression of BMX and α-SMA was detected in GBM specimens with high pericyte coverage relative to the GBMs with low pericyte coverage. (n = 5 specimens for each group; **, $p < 0.01$; mean ± s.e.m.; Mann Whitney test).

(D) Immunofluorescent staining of BMX (in green) and the pericyte marker Desmin (in red) in the differentiated cells derived from T3832 and CCF3264 GSCs. GSCs were cultured in DMEM supplemented with 10% FBS for 5 days to achieve differentiation. BMX signals were detected in pericyte-like cells (Desmin+) in vitro. Scale bar represents 40μm.

(E) Statistical quantification of (D) shows the percentage of BMX positive staining in Desmin+ pericyte-like cells in vitro in differentiated glioma cells. More than 80% of the Desmin+

pericyte-like cells also showed BMX expression (n = 100 cells for each group; three independent replicates; *, $p < 0.05$; mean ± s.e.m.; Mann Whitney test).

(F) Immunofluorescent analysis of BMX (in green) and the endothelial marker Glut1 (in red) in xenografts derived from GSCs transduced with DesPro-HsvTK or DesPro-Vec control after GCV treatment. GCV treatment reduced BMX signals surrounding the vessels in xenografts derived from the DesPro-HsvTK-transduced GSCs relative to xenografts derived from the DesPro-Vec-transduced GSCs. As GCV treatment selectively targets GSC-derived pericytes expressing HsvTK, the loss of BMX signal surrounding the vessels confirmed that GSC-derived neoplastic pericytes express BMX. However, in the non-vessel areas, the BMX+ population (GSCs) was not affected by the disruption of GSC-derived pericytes. Scale bar represents 40μm.

(G) Statistical quantification of the percentage of BMX+ cells in vascular and perivascular regions in xenografts derived from the GSCs transduced with DesPro-Vec or DesPro-HsvTK after GCV treatment. BMX+ cells in the vascular and perivascular areas (in the proximity of vessels within 100μm) were analyzed. Percentage of BMX+ cells was significantly reduced in xenografts derived from GSCs transduced with DesPro-HsvTK relative to xenografts derived from the GSCs transduced with DesPro-Vec control after GCV treatment (n = 5 tumors for each group; **, $p < 0.01$, mean ± s.e.m.; Mann Whitney test).

(H and I) Immunofluorescent staining of the tight junction markers ZO-1 (H) and Occludin (I) (in green) and the endothelial marker Glut1 (in red) in orthotopic xenografts derived from GSCs (T4121) expressing shNT or shBMX. A reduced ZO-1 and Occludin expression on vessels was detected in xenografts derived from shBMX-expressing GSCs relative to xenografts derived from shNT-expressing GSCs, which was reminiscent of the loss of tight junctions in xenografts with pericyte disruption. Scale bar represents 80μm.

(J and K) Statistical quantification of (H and I) to determine the ZO-1 (J) and Occludin (K) signals on vessels in xenografts derived from GSC expressing shNT or shBMX. Percentage of ZO-1- and Occludin-positive vessels was determined by the numbers of ZO-1- and Occludin-positive cells normalized to the numbers of Glut1-positive cells (n = 5 tumors for each group; *, $p < 0.05$; mean ± s.e.m.; Mann Whitney test).

Figure S7. Targeting GSC-derived Pericytes Improved Chemotherapy Efficacy in GBMs with Low Pericyte Coverage, Related to Figure 7.

(A) *In vivo* bioluminescent imaging of intracranial tumor growth in mice bearing GBMs derived from UCG163 GSCs after treatment with etoposide, ibrutinib, etoposide plus ibrutinib, or DMSO control. Orthotopic GBM xenografts derived from UCG163 GSCs have relatively low pericyte coverage (Fig. S6C). Mice bearing the tumors were treated with DMSO control, etoposide, ibrutinib, or etoposide plus ibrutinib. The treatments started on day 7 after post-transplantation. Representative images on day 7, day 15 and day 30 post-transplantation of GSCs were shown. Etoposide or ibrutinib treatment alone showed some modest inhibition of tumor growth, but the etoposide plus ibrutinib treatment achieved maximal inhibition of tumor growth.

(B) Kaplan-Meier survival curves of mice bearing GBMs derived from UCG163 GSCs after treatment with etoposide, ibrutinib, etoposide plus ibrutinib, or DMSO control. Etoposide or ibrutinib treatment alone significantly extended animal survival. However, etoposide plus ibrutinib treatment achieved the longest survival of animals among the four groups (n = 5 mice for each group; *, $p < 0.05$; **, $p < 0.01$; two-tailed log-rank test).

(C) *In vivo* bioluminescent imaging of intracranial tumor growth in mice bearing the orthotopic xenografts derived from UCG163 GSCs transduced with DesPro-Vec or DesPro-HsvTK after

treatment with GCV in combination with etoposide or DMSO. Mice bearing the tumors were treated with etoposide or DMSO control along with pulse GCV treatment. The treatments started on day 7 after transplantation. Representative images on day 7, day 15 and day 30 post-transplantation of GSCs were shown. Etoposide treatment or disrupting GSC-derived pericytes by GCV showed some inhibition of tumor growth, but etoposide treatment plus disruption of GSC-derived pericytes by GCV achieved the maximal inhibition of tumor growth in xenografts derived from the DesPro-HsvTK-transduced GSCs.

(D) Kaplan-Meier survival curves of mice bearing GBMs derived from UCG163 GSCs transduced with DesPro-Vec or DesPro-HsvTK after treatment described in (C). Etoposide treatment or disrupting GSC-derived pericytes by GCV significantly extended animal survival. However, etoposide plus disruption of GSC-derived pericytes by GCV achieved the longest survival of mice bearing the xenografts derived from the DesPro-HsvTK-transduced GSCs (n = 5 mice for each group; *, $p < 0.05$; **, $p < 0.01$; two-tailed log-rank test).

Table S1. Information about the Primary GBM Patients in This Study, Related to Figure 1.